Atomic Decoration for Improving the Efficiency of Field Electron Emission of Carbon Nanotubes

Guihua Chen, Zhibing Li,*,† Jie Peng, Chunshan He, Weiliang Wang, Shaozhi Deng, and Ningsheng Xu*,‡

State Key Laboratory of Optoelectronic Materials and Technologies School of Physics and Engineering, Sun Yat-Sen University, Guangzhou 510275, China

Chongyu Wang and Shanying Wang

Department of Physics, Tsinghua University, Beijing 100084, China

Xiao Zheng and GuanHua Chen

Department of Chemistry, the University of Hong Kong, Hong Kong, China

Tao Yu

Central Iron and Steel Research Institute, Beijing, China

Received: September 26, 2006; In Final Form: February 5, 2007

The field electron emission from the single-walled carbon nanotubes with their open ends terminated by $^{-}$BH, $^{-}$NH, and $^{-}$O has been simulated. We find that $^{-}$BH and $^{-}$NH suppress the apex−vacuum barrier significantly and lead to higher emission current in contrast to the $^{-}$O-terminated structure. The calculated binding energy implies that the carbon nanotubes terminated with $^{-}$BH and $^{-}$NH are more stable than those saturated by oxygen atoms or by hydrogen atoms. The simulation shows that the most probable orientation of the emission beam has correlation to the atomic structure of the apex and is field-dependent.

I. Introduction

The field electron emission (FE) from carbon nanotubes (CNTs) has found its applications in flat panel displays[1] and in molecular sensors.[2−4] It has also shown potential applications in miniature highbrightness electron sources for electron microscope[5] and in parallel e-beam lithography systems.[6] One of the central problems in these applications is to optimize the structure to achieve stronger FE in lower macroscopic field. It was once believed that the large aspect ratio of a CNT that would lead to large local field enhancement (LFE) at the apex of the CNT was the major reason responsible for the superior FE, hence it would be straightforward to improve the FE efficiency by increasing the length of the CNT. But this common view has not been verified satisfactorily by either experimental or theoretical studies. Recent simulations have shown that the charge accumulation in both the apex and the body of the CNT can significantly modify the apex−vacuum barrier (AVB) and thereby the FE characteristics.[7,8] A recent simulation found that the field enhancement factor for the open single-walled CNT (SWCNT) is much smaller than the expected value of the metal rod model; on the other hand, the change of the AVB has a more pronounced effect on FE.[9]

Since a CNT emitter has only decades of atoms at the apex, the atomic structure of the apex would have strong influence on the FE process. The following effects have been observed in experiments: the hydrogenation of the tube wall transforms a metallic CNT to a semiconductive one,[10] O_2 exposure increases the turn-on field of SWCNTs and decreases the FE efficiency,[11] and the adsorption of H_2O enhances the field emission current.[12] However, experimental observations for the adsorbate effects so far have not been conclusive.[11,13,14] To understand the dependence of FE upon the atomic structure of the apex, careful simulations via the density functional method (DFT) have been carried out.[15−21] However, there are contradictory conclusions about the effect of adsorbates. Zhou et al.[22] and Kim et al.[7,23] obtained the local density of states (LDOS) at the apex by the ab initio methods and found that the LDOS at the charge-neutrality level is suppressed by the hydrogen. They therefore concluded that hydrogen adsorption reduces the FE current density. By contrast, Mayer et al. calculated the AVB using a dipole and point charge model.[7] They acclaimed that the apex−vacuum barrier is reduced by the presence of the hydrogen, and thereby concluded that hydrogen adsorption would enhance the FE current density. Mayer recently improved the model and illustrated the electrostatic potential around the carbon nanotube.[10] More careful studies on this topic would obviously be useful.

Only recently has it been possible to tackle the SWCNT of realistic size in the FE conditions by a multiscale method involving quantum mechanics and molecular mechanics.[8,24] In the present paper, we have adopted this method to simulate the FE from the SWCNT of realistic length (one micrometer) with different atomic decorations at the open end of the tube. Obviously the AVB and thereby the FE characteristic will be strongly affected by the electron transfer between the carbon atoms and the adsorbent atoms. The atomic decoration in the

* Address correspondence to this author.
† E-mail: stslzb@mail.sysu.edu.cn.
‡ E-mail: stsxns@mail.sysu.edu.cn.

10.1021/jp066316w CCC: $37.00
Published on Web 03/09/2007

TABLE 1: Electronegativity of Related Atoms in the Allen Electronegativity Scale

	H	B	C	N	O
X_S	2.300	2.051	2.544	3.066	3.610

apex will induce dipoles due to the geometric symmetry breaking in the axial direction. If the dipole has its positive end outward to the vacuum (positive dipole), it tends to suppress the AVB; otherwise (negative dipole), it inclines to raise the barrier. This simple argument suggests that the carbon dangling bonds in the open end of the SWCNT should be saturated by atoms with electronegativity (X_S) lower than that of the carbon atom. For instance, the hydrogen-terminated SWCNT has a positive dipole because hydrogen has lower X_S than carbon.[9] The electronegativities of hydrogen, boron, carbon, nitrogen, and oxygen in the Allen electronegativity scale are given in Table 1.

At room temperature, the electrons in the vicinity of the apex are most relevant to the emission. When the apex has a higher density of electrons, there are more incident electrons hitting on the AVB and a stronger emission current could be expected. To attract electrons from the tube column to the apex, it would be useful to saturate the CNT first by atoms of higher X_S followed by atoms of lower X_S. Another consideration is the structural stability that is one of the properties of most concern in the applications. In this paper, we should consider the diatom ions $^-$BH and $^-$NH as adsorbates and compare them with the oxygen ion. Our simulation should show that the adsorbates of $^-$BH and $^-$NH have larger binding energy than both oxygen and hydrogen.

We should adopt the multiscale method[8,24] to simulate the (5, 5) SWCNT with its open end saturated in three kind of ions: $^-$BH, or $^-$NH, or $^-$O. In Section II, the method of simulation is reviewed briefly. The charge density and electrostatic potential in the absence of applied field is given in Section III. In Section IV, the field-dependent AVB is illustrated. The most probable emission path is studied and the emission characteristics of the (5, 5) SWCNTs saturated with $^-$BH, $^-$NH and $^-$O are presented in Section V. The last section is devoted to the discussion and conclusions.

II. Simulation Method and the Ending Structures

The concept of multiscale coupling is important for the simulation of huge systems that are sensitive to all scales of the systems.[25,26] The CNTs for the purpose of FE are typical multiscale systems. A simplified schematic setup of the FE system is shown in Figure 1, in which two black plates are the cathode (left) and anode (right); a CNT is mounted vertically on the cathode. When a voltage is applied to the two metal plates, the electrons have opportunity to emit into vacuum through the apex of the CNT by quantum tunneling.

In experiments, the length of CNTs is usually in micrometers, while the radius is in nanometers. For instance, the (5, 5) type SWCNT of 1 μm length consists of about 10 000 carbon atoms. Limited by the computational efficiencies and resources, all ab initio studies so far can only simulate the local properties involving hundreds of carbon atoms. As the electronic properties are sensitive to both the detailed atomic arrangement (i.e., the location of defects and adsorbates) and the electron states, which would extend through the whole tube, it is a big challenge to simulate the whole tube that has a length on the micrometer scale.

Since electrons are emitted from the apex of the SWCNT by quantum tunneling, the apex part must be treated by quantum

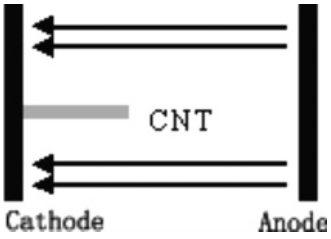

Figure 1. The schematic setup of field electron emission. The arrow lines represent the applied electric field.

mechanics. The part on the substrate side mainly affects the FE through Coulomb potential of the excess charge, so that it can be treated by a semiclassical method.[8,24] Therefore we divide the SWCNT into a quantum region and a semiclassical region. The quantum region is simulated on the atomic scale where the density matrix of electrons is obtained quantum mechanically. In the semiclassical region, the Coulomb potential is governed by Poisson's equation.

It should be noted that even in the semiclassical region the electron energy band structure originating from quantum mechanics should be taken into account. The excess charge distribution in the semiclassical region has a simple solution only for the simple band structure. For the (5, 5) SWCNT, there is both experimental and theoretical evidence for the constant density of states (DOS) in the vicinity of the neutrality level.[27−30] Hence the semiclassical region should be limited in the region where the constant DOS is valid. In our experience, this means that the length of the quantum region should be over 100 nm.

In the present simulation, the quantum region extends 123 nm and contains 10000 atoms. It is still too big for an ab initio simulation. The quantum region is then further divided into subregions. Each subregion together with its adjacent subregions as buffer forms a subsystem that is simulated by the modified neglect of diatomic overlap (MNDO) semiempirical quantum mechanical method (here the MOPAC software has been used). The excess charges in the quantum region but not in the subsystem being simulated are treated as point charges. Their contribution to the subsystem being simulated is through the Coulomb interaction.

The coupling of the quantum region and the semiclassical region is through the quasithermodynamic equilibrium condition, which assumes that the electrochemical potential (Fermi level) is a constant along the nanotube, and equal to that of the substrate. The densities of the excess charge ("excess density" for simplicity) calculated separately in quantum and semiclassical regions should coincide at some overlap place of two regions. Here we required that the excess densities coincide at a position 900 nm from the substrate. The self-consistent excess density of the entire CNT is achieved through iterations that contain a small loop and a big loop. In the small loop, the subregions of the quantum region are simulated one by one, and repeated until a converged electron density of the quantum region is obtained. In the big loop, the quantum region and the semiclassical region are simulated alternately until the self-consistent charge distribution is achieved. This process is greatly accelerated by the observation that the charge density in the region far from the apex, to a good approximation, is a linear function of the distance from the substrate. This linear behavior is a consequence of the constant DOS in the classical region.[31]

When the SWCNT is mounted on the metallic substrate, a Schottky junction will be formed at the back contact in principle. However, as the SWCNT here is very long, the effect of this junction could be ignored. Equivalently, we have assumed that the Fermi level of the isolated SWCNT aligns with that of the

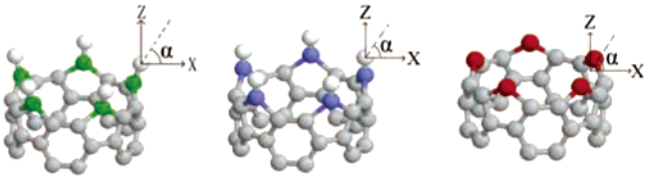

Figure 2. Three ending structures of the (5, 5) SWCNT. The gray balls stand for carbon atoms. (a) The a-type structure with $^{-}$BH as adsorbates. The green balls stand for boron atoms and the white balls for hydrogen atoms. (b) The b-type structure with $^{-}$NH as adsorbates. The blue balls and the white balls denote nitrogen atoms and hydrogen atoms, respectively. (c) The c-type structure with oxygen ions as adsorbates. The red balls stand for oxygen atoms. The *Z*-axis in each figure is parallel to the axis of the tube. The *X*-axis is the radial axis on the plane perpendicular to the tube axis and through a hydrogen atom (for Figure 2, parts a and b) or through the middle point of two adjacent oxygen atoms (for Figure 2c). The angle α is on the *X*−*Z* plane.

TABLE 2: The Coordinates of the Adsorbates and the Carbons of the Top Layer[a]

		coordinate (Å)		
structures	atoms	*Z*	*X*	*Y*
$^{-}$BH	H	10088.04	2.35	2.85
	B	10086.92	2.10	2.53
	C	10086.04	0.94	3.31
$^{-}$NH	H	10087.60	2.35	2.83
	N	10086.87	1.91	2.31
	C	10086.04	0.94	3.31
$^{-}$O	O	10086.83	2.05	2.46
	C	10086.04	0.94	3.31

[a] *Z* stands for the axial coordinate with the origin on the substrate surface, *X* and *Y* denote two orthogonal coordinates of the plane perpendicular to the tube axis, with the origin at the axis.

metal. The boundary condition of the metal surface is guaranteed by the image charges of the excess charges of the SWCNT. The total electrostatic potential is the superposition of the Coulomb potential created by excess charges and their images in the substrate, as well as the applied macroscopic field.

The apex structures with $^{-}$BH, $^{-}$NH, and $^{-}$O terminations are shown in Figure 2; they are referred to as a-type, b-type, and c-type structures, respectively. The five green balls in Figure 2a for the a-type structure stand for the boron atoms. Each boron atom shares two bonds with two carbon atoms. The third bond of the boron atom is saturated by a hydrogen atom (the white ball). Similarly, the b-type structure is shown in Figure 2b, with the blue balls for nitrogen atoms and the white balls for hydrogen atoms. The five oxygen atoms are represented by red balls in Figure 2c for the c-type structure. All ending structures are relaxed with the MOPAC software. The coordinates of adsorbent atoms and the first layer of carbons are given in Table 2.

The binding energy E_{bind} is defined as

$$E_{bind} = E_{sep} - E_{bond} \quad (1)$$

where E_{sep} is the total energy of the system in which the adsorbates are separated far away from each other and from the CNT, and E_{bond} is the total energy of the system in which the adsorbates are bonding with the carbons of the top layer. In the calculation of binding energies, we only consider the last ten layers of carbons at the tip. The stability of the ending structure is described by the binding energy per adsorbent diatom of the a-type/b-type structure or per adsorbent atom for the c-type structure. The results are given in Table 3. The a-type and b-type ending structures are more stable than the c-type structure and the structure in which every dangling bond of carbon is saturated by a hydrogen atom.

TABLE 3: The Binding Energy of Adsorbates

	$^{-}$BH	$^{-}$NH	$^{-}$O	$^{-}$H
binding energy (eV)	17.8	18.3	3.99	8.63

III. Electronic Structures in the Absence of Applied Field

The FE characteristic of each individual SWCNT should rely on its intrinsic electronic structure. Therefore in this section we focus on the electronic structures of the SWCNT in the absence of external macroscopic field.

Figure 3a−c shows the electron density in the intersection plane, on which the axis of SWCNT and one boron (a)/nitrogen (b)/oxygen (c) atom are located. The arrows mark the positions of the adsorbent atoms. In the a-type structure (Figure 3a), electrons obviously transfer from the boron atoms to the hydrogen atoms. From Figure 3b, one can see that electrons in the b-type structure are concentrated at the nitrogen atoms. The electrons are strongly concentrated at the oxygen atoms in the c-type structure (Figure 3c). The electron distribution in the c-type structure can be seen more clearly in Figure 4, where the distribution of excess electrons is shown along the wall of the SWCNT. The excess charge associated with each atom of the top three (two) layers in the a-type/b-type (c-type) structure has been calculated by the Mulliken population analysis method. The results are given in Table 4. Since the boron has smaller electronegativity compared with the carbon and the hydrogen, electrons tend to transfer from the boron to both the carbon and the hydrogen in the a-type structure and lead to a dipole with its negative charge outward. In the c-type structure, we find a dipole of the same direction as the dipole in the a-type structure with a bigger value. This is expected as X_S of the oxygen is much larger than that of the carbon. A reversed dipole, i.e., with its positive charge outward, arises in the b-type structure due to the large electronegativity of the nitrogen. The dipole values of the top three (two) layers of the a-type and b-type (c-type) structures are given in Table 5.

IV. Field-Dependent Barrier

Now let us investigate the response of the SWCNT to the macroscopic fields (F_{appl}). The general picture is as follows. The applied field F_{appl} drives electrons to the tip of the SWCNT until the equilibrium is set up. We assume that the emission current is weak and can be ignored in the calculation of the electron density of the SWCNT. The redistribution of electrons in F_{appl} has two consequences. First, the field is more or less shielded in the body of the tube. This leads to the field enhancement at the apex. However, as the wall of the SWCNT has only one layer of atoms, the shielding would not be complete, especially in the apex region where the field is strong. There would be a field penetration in the apex region, so the field enhancement factor is smaller than that predicted by the classical theory for a metal rod. Second, there are excess charges accumulating along the tube, especially in the apex region. In the quasiequilibrium assumption, the charge accumulation is possible only if the neutrality energy level of the SWCNT bends down. This happens when the applied field lowers the energies of local orbitals so that the orbitals with their energies lying between the Fermi level of the substrate and the neutrality energy level can accommodate electrons and contribute to excess charges.

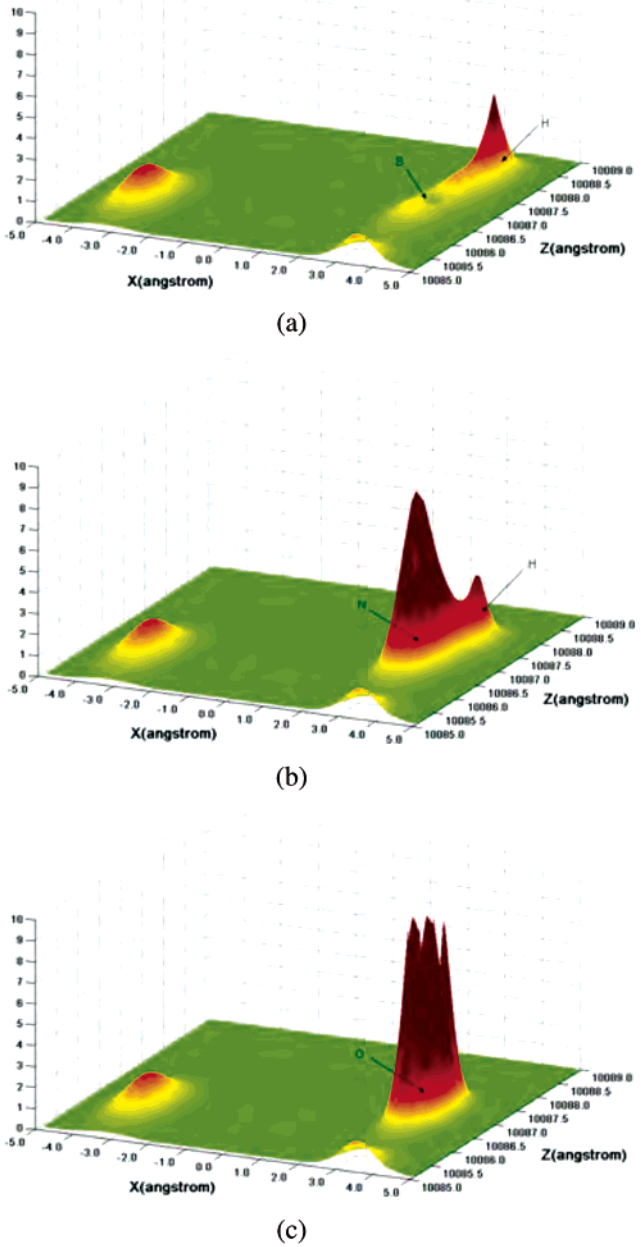

Figure 3. The distribution of electrons on the intersection plane crossing one adsorbate atom and the axis of the SWCNT. Parts a, b, and c correspond to the a-type, b-type, and c-type structures, respectively.

The superposition of Coulomb potential of all charges in the tube and their images in the substrate, together with the potential of F_{appl}, determines the AVB for the electron emission. In Figure 5a, we plot the electrostatic potential $U(z)$ of the a-type structure for various F_{appl}. The Z axis has its origin at the last atom of the SWCNT and is parallel to the direction of the tube axis. The dependence of AVB on F_{appl} is remarkable. The barrier potentials $U(z)$ of the three ending structures are compared in Figure 5b for 7.0 V/μm. Compared to the AVB of the a-type structure, the AVB of the b-type structure is lower but thicker. This partly results from the difference of the apex dipoles (see Table V). Suppose that the applied field would not change significantly the intrinsic electronic structure of the SWCNT. Then in the a-type (b-type) structure, the atoms of the first layer

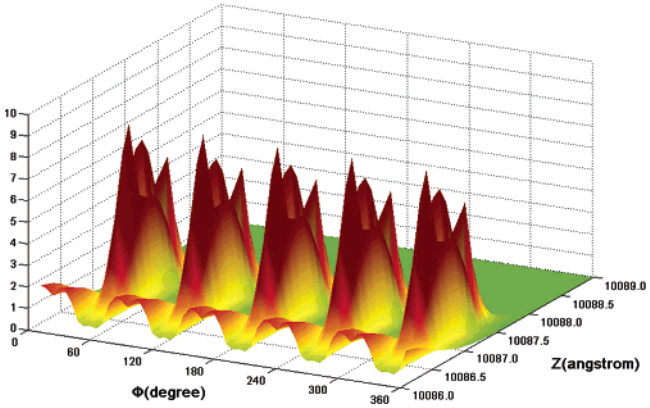

Figure 4. The electron distribution around the atoms of the last two layers of the SWCNT terminated with oxygen atoms.

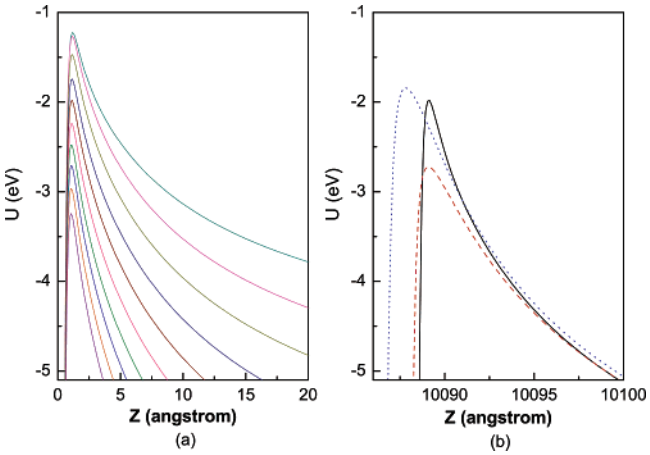

Figure 5. The AVB of the SWCNT. (a) $U(z)$ of the a-type structure with F_{appl} from 6.0 to 15.0 V/μm, by steps of 1.0 V/μm. The origin is at one of the last nucleui of the SWCNT. The lower barrier corresponds to larger F_{appl}. (b) $U(z)$ of the three ending structures in the applied field of 7.0 V/μm. The solid, dashed, and dotted curves correspond to the a-type, b-type, and c-type structures, respectively. Here the origin is on the surface of the substrate.

TABLE 4: The Distribution of the Excess Charges

atom group	excess charges (e)
CBH	−0.082 (C), 0.276 (B), −0.039 (H)
CNH	0.086 (C),−0.248 (N), 0.150 (H)
CO	0.182 (C),−0.302 (O)

TABLE 5: The Dipoles in the First and the Second Top Layers

	dipole (e•nm)	
structures	atom of first layer	atom of second layer
$^{-}$BH	−0.0095	0.0135
$^{-}$NH	0.0158	−0.0122
$^{-}$O	−0.0154	−0.0051

have negative (positive) dipoles, and the atoms of the second layer have positive (negative) dipoles. The potential close to the apex is mostly affected by the atoms of the first layer and is enhanced (suppressed). Apart from the apex in some distance (7 Å), the dipoles of the first layer would be screened by those of the second layer, and the potential of the a-type structure could not be distinguished from that of the b-type. For the c-type structure, the dipoles of the first two layers are negative, and the net negative dipole and the large negative excess charge at the apex make the AVB high and thick.

The field enhancement factor as a feature of the AVB is of great concern in the FE applications. For the SWCNT, however,

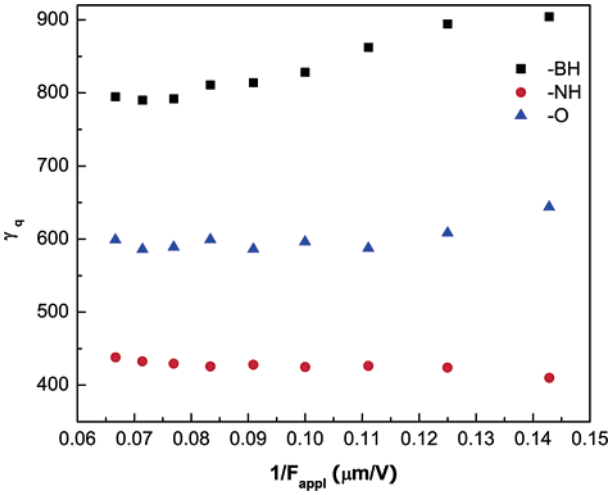

Figure 6. The field enhancement factor versus the inverse of applied field. The squares, circles, and triangles are data of the simulations of the a-type, b-type, and c-type structures, respectively.

it is difficult to define a quantity that corresponds exactly to the field enhancement factor as usually defined for planar metallic emitters. Denote the maximum local field by F_{apex}. Here the field enhancement factor γ_q is defined as F_{apex}/F_{appl}. The variation of this field enhancement factor with the value of $1/F_{appl}$ is shown in Figure 6. Note that γ_q values of these structures do not change significantly with applied fields, but are obviously different from each other. This reflects the important influence of the adsorbates on FE.

V. Emission Currents and Emission Paths

According to quantum mechanics, electrons may emit to the vacuum along any path with nonzero probability. In the semiclassical approximation, only the path of the least (maximum) action is considered. This path will be referred to as the most probable path (MPP). Since the a-type and b-type ending structures have the thinnest AVB in front of the hydrogen atoms, MPP of these structures should start from the hydrogen atom. The thinnest AVB of the c-type structure starts from the top carbon atoms and goes outward along a path through the middle point of two adjacent oxygen atoms. For simplicity, we assumed that the electrons go through the barrier in straight lines. The path angles (α) of three ending structures are presented schematically in Figure 2. Along the MPP, the transmission coefficient (D) can be estimated by the WKB approximation

$$D = \exp\left[-\frac{2}{\hbar}\int\sqrt{2mV(z)}\,dz\right] \quad (2)$$

where $V(z)$ is the electron energy potential related to the Fermi level, and the integral is over the classical forbidden region, i.e., where $V(z) > 0$. We have assumed that the electrons possess the Fermi level. If the path is not the MPP, the value of D by eq 2 should be smaller. For instance, in Figure 7, D is plotted against the path angle for the a-type structure in 12.0 V/μm. The angle of the MPP is determined by the maximum of D. Since the AVB is field-dependent, the MPP would change its orientation with the applied fields. The angles of the MPP versus the applied fields are plotted in Figure 8. The squares, circles, and triangles correspond to the a-type, b-type, and c-type structures, respectively. One sees that the angle of the MPP decreases as the applied field increases. This phenomenon would be related to the fact that higher applied field induces more excess electrons at the apex.

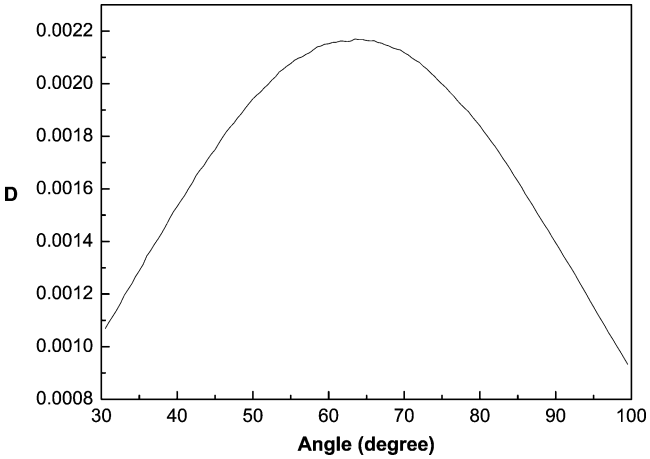

Figure 7. D versus path angle for the a-type structure in 12.0 V/μm.

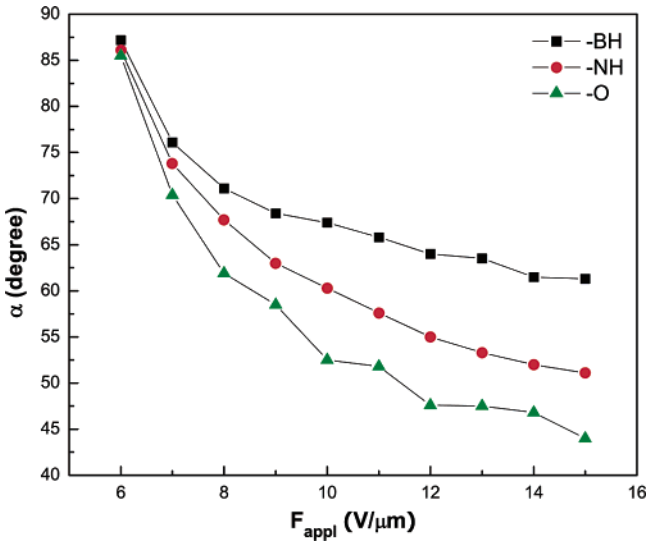

Figure 8. The angle of the most probable path versus the applied field. The squares, circles, and triangles are the data corresponding to the a-type, b-type, and c-type structures, respectively.

With D in hand, the emission current is estimated by

$$I = \nu q_{exc} D \quad (3)$$

where q_{exc} are the excess electrons around the atoms from which the MPPs start, and ν is the collision frequency that can be estimated from the average kinetic energy of π^* electrons as $E_k(\pi^*)/h$. Another way to estimate the collision frequency is to use the uncertainty relation

$$\nu = \frac{E_k}{h} = \frac{h}{32\pi^2 m\langle\Delta r^2\rangle} \quad (4)$$

where $\langle\Delta r^2\rangle$ is the uncertainty of the radial coordinate. Its numerical value can be estimated from the density of excess electrons (Figure 3). The collision frequency estimated by two methods has the same order of 10^{14} Hz.

The diagram of the emission current versus applied field is presented in Figure 9, where squares, circles, and triangles are for the a-type, b-type, and c-type structures, respectively. For each structure, the emission current is the summation of the currents along five MPPs, with each MPP as defined in Figure 2.

To confirm that the emission is dominated by the MPPs, we have also calculated the emission current along the path starting

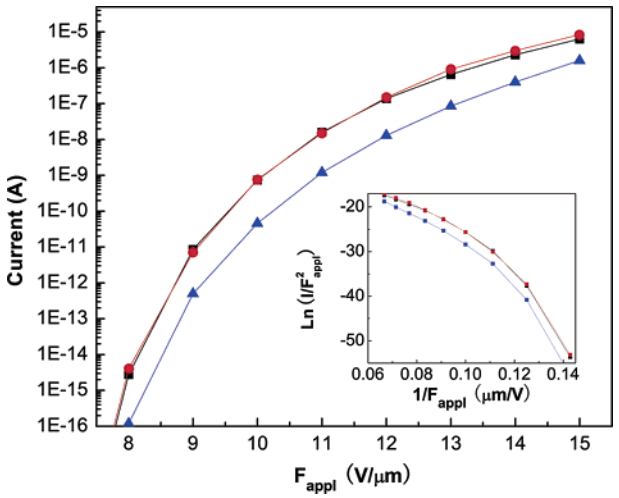

Figure 9. The current versus applied field. The squares, the circles, and the triangles are the currents corresponding to the a-type, b-type, and c-type structures, respectively. The inset is the Fowler−Nordheim plot where $1/F_{appl}$ is the horizontal axis and $\log(I/F_{appl}^2)$ the vertical axis.

TABLE 6: The Emission Currents (A) from the MPP and from the Path in between Two MPPs

	$^-$BH	$^-$NH	$^-$O
MPP	1.4×10^{-7}	1.5×10^{-7}	1.3×10^{-8}
path not a MPP	8.7×10^{-9}	1.4×10^{-8}	2.1×10^{-9}

from a charge center in between two nearby MPPs. The results for $F_{appl} = 12.0$ V/μm are compared in Table 6. The contribution of the MPP is one order or so larger than that of not a MPP.

VI. Conclusions and Discussions

A 1 μm long (5, 5) single-walled carbon nanotube (SWCNT) has been simulated by the multiscale method, with the interest focused at the effects of the ending structures. The apex−vacuum barriers of the SWCNTs ended by $^-$BH, $^-$NH, and $^-$O respectively have been obtained. The local field enhancement factor is different from one ending structure to another; all are much smaller than the prediction of the classical model. The lowering of the apex−vacuum barrier by the applied field, besides the local field enhancement, as the essential mechanism is confirmed to be responsible for the low turn-on field of SWCNTs.

According to our simulations, the SWCNTs terminated with diatoms whose outer atoms have smaller electronegativity would be superior in field emission and have a more stable structure. The turn-on field (11.5 V/μm) of the SWCNT terminated with $^-$BH or $^-$NH is smaller than that terminated by oxygen. In the same applied field, the current of oxygen terminated SWCNT is an order or more weaker than those terminated by $^-$BH and $^-$NH. The simulation suggests that the binding energy of the diatom decorated SWCNTs is about 4.5 times the binding energy of the oxygen-saturated SWCNT and more than double that of the hydrogen-saturated one. The electronegativity of the adsorbates may partly explain the feature of the apex−vacuum barrier and give a general hint for the structure optimization. The orientation of the most probable emission path depends on the applied field significantly. This observation would provide a means for extracting the atomic features of the apex.

One can see that the best turn-on field we estimated for the $^-$BH ending structure is still larger than most experimental results, which is about 1−5 V/μm.[32] There are a number of reasons for this, besides the uncontrollable error of the simulation. First, the emission current could be larger if one takes into account the emission from the paths other than the most probable paths we have considered. Second, in our calculation, we have ignored the exchange and correlation effect (i.e., the image force) on the emitting electron. The prediction would be improved by including this effect. However, to our knowledge, it is still difficult to include the exchange and correlation effect in a quantum mechanical simulation of emission current of SWCNT.[33] Last but not least, most, if not all, CNTs used in the FE experiments are multiwalled CNTs and the chirality is not controllable. The experimentally observed emission current would be higher since the multiwalled CNTs would have a larger field enhancement factor as would resemble more a classical metal rod. The above argument implies the existence of a discrepancy between our simulational result and the experimental observations. Optimistically, our simulation would have revealed some virtual elements involved in the field emission of SWCNT with the atomic decoration, at least qualitatively.

Acknowledgment. The authors thank Chris J. Edgcombe and Richard G. Forbes for valuable discussions and gratefully acknowledge the support from the National Natural Science Foundation of China (the Distinguished Creative Group Project, Grant Nos. 10674182, 90103028, and 90306016) and from Hong Kong Research Grant Council (HKU 7010/03P and HKU 7012/04P).

References and Notes

(1) Choi, W. B.; Chung, D. S.; Kang, J. H.; Kim, H. Y.; Jin, Y. W.; Han, I. T.; Lee, Y. H.; Jung, J. E.; Lee, N. S.; Park, G. S.; Kim, J. M. *Appl. Phys. Lett.* **1999**, *75*, 3129.

(2) Collins, P. G.; Bradley, K.; Ishigami, M.; Zettl, A. A. *Science* **2000**, *287*, 1801−1804.

(3) (a) Kong, J.; Franklin, N. R.; Zhou, C.; Chapline, M. G.; Peng, S.; Cho, K.; Da, H. *Science* **2000**, *287*, 622−625 (b) Peng, S.; Cho, K. *Nanotechnology* **2000**, *11*, 57−60.

(4) Chang, H.; Lee, J. D.; Lee, S. M.; Lee, Y. H. *Appl. Phys. Lett.* **2001**, *79*, 3863−3865.

(5) Jonge, N.; Lamy, Y.; Schoots, K.; Oosterkmp, T. H. *Nature* (*London*) **2002**, *420*, 393.

(6) Semet, V.; Binh, V. T.; Vincent, P.; Guillot, D.; Teo, K. B. K.; Chhowalla, M.; Amaratunga, G. A. J.; Milne, W. I.; Legagneux, P.; Pribat, D. *Appl. Phys. Lett.* **2002**, *81*, 343.

(7) Mayer, A.; Miskovsky, N. M.; Cutler, P. H.; Lambin, Ph. *Phys. Rev. B* **2003**, *68*, 235401.

(8) Zheng, X.; Chen, G. H.; Li, Z.; Deng, S.; Xu, N. *Phys. Rev. Lett.* **2004**, *92*, 106803.

(9) Peng, J.; Li, Z.; He, C.; Chen, G.; Wang, W.; Deng, S.; Xu, N.; Zheng, X.; Chen, G.; Edgcombe, C.; Forbes, R. e-print cond-mat/0612600.

(10) Lee, S. M.; An, K. H.; Lee, Y. H.; Seifert, G.; Frauenheim, T. *J. Am. Chem. Soc.* **2001**, *123*, 5059−5063.

(11) Wadhawan, A.; Stallcup, R. E., II; Stephens, K. F., II; Perez, J. M.; Akwani, I. A. *Appl. Phys. Lett.* **2001**, *79*, 1867.

(12) Maiti, A.; Andzelm, J.; Tanpipat, N.; Allmen, P. *Phys. Rev. Lett.* **2001**, *87*, 155502.

(13) Zhi, C. Y.; Bai, X. D.; Wang, E. G. *Appl. Phys. Lett.* **2002**, *81*, 1690.

(14) Kim, C.; Seo, K.; Kim, B.; Park, N.; Choi, Y. S.; Park, K. A.; Lee, Y. H. *Phys. Rev. B* **2003**, *68*, 115403.

(15) Jhi, S.-H.; Louie, S. G.; Cohen, M. L. *Phys. Rev. Lett.* **2000**, *85*, 1710.

(16) Zhu, X. Y.; Lee, S. M.; Lee, Y. H.; Frauenheim, T. *Phys. Rev. Lett.* **2000**, *85*, 2757.

(17) (a) Liang, W. Z.; Yokojima, S.; Zhou, D. H.; Chen, G. H. *J. Phys. Chem. A* **2000**, *104*, 2445. (b) Liang, W. Z.; Wang, X. J.; Yokojima, S.; Chen, G. H. *J. Am. Chem. Soc.* **2000**, *122*, 11129. (c) Liang, W. Z.; Yokojima, S.; Ng, M. F.; Chen, G. H.; He, G. *J. Am. Chem. Soc.* **2001**, *123*, 9830.

(18) (a) Park, N.; Han, S.; Ihm, J. *Phys. Rev. B* **2001**, *64*, 125401. (b) Sorescu, D. C.; Jordan, K. D.; Avouris, Ph. *J. Phys. Chem. B* **2001**, *105*, 11227.

(19) Sorescu, D. C.; Jordan, K. D.; Avouris, Ph. *J. Phys. Chem. B* **2001**, *105*, 11227.

(20) Moon, C.-Y.; Kim, Y.-S.; Lee, E.-C.; Jin, Y.-G.; Chang, K. J. *Phys. Rev. B* **2002**, *65*, 155401.

(21) Steckel, J. A.; Jordan, K. D.; Avouris, Ph. *J. Phys. Chem. A* **2002**, *106*, 2572.
(22) Grujicic, M.; Cao, G.; Gersten, B. *Appl. Surf. Sci.* **2003**, *206*, 167.
(23) Zhou, G.; Duan, W.; Gu, B. *Phys. Rev. Lett.* **2001**, *87*, 095504.
(24) Kim, C.; Choi, Y. S.; Lee, S. M.; Park, J. T.; Kim, B.; Lee, Y. H. *J. Am. Chem. Soc.* **2002**, *124*, 9906.
(25) Peng, J.; Li, Z.; He, C.; Deng, X.; Xu, N.; Zheng, X.; Chen, G. H. *Phys. Rev. B* **2005**, *72*, 235106.
(26) Fu, C.-C.; Torre, J. D.; Willaime, F.; Bocquet, J.-L.; Barbu, A. *Nature* (*London*) **2005**, *4*, 68.
(27) Chang, R.; Ayton, G. S.; Voth, G. A. *J. Chem. Phys.* **2005**, *122*, 244716.
(28) Rao, A. M.; Richter, E.; Bandow, S.; Chase, B.; Eklund, P. C.; Williams, K. A.; Fang, S.; Subbaswamy, K. R.; Menon, M.; Thess, A.; Smalley, R. E.; Dresselhaus, G.; Dresselhaus, M. S. *Science* **1997**, *275*, 187.
(29) Blase, X.; Benedict, L. X.; Shirley, E. L.; Louie, S. G. *Phys. Rev. Lett.* **1994**, *72*, 1878.
(30) Jishi, R. A.; Bragin, J.; Lou, L. *Phys. Rev. B* **1999**, *59*, 9862.
(31) Wilder, J. W. G.; Venema, L. C.; Rinzler, A. G.; Smalley, R. E.; Dekker, C. *Nature* (*London*) **1998**, *391*, 59.
(32) Li, Z.; Wang, W. *Chin. Phys. Lett.* **2006**, *23*, 1618.
(33) Xu, N. S.; Huq, S. E. *Mater. Sci. Eng., R* **2005**, *48*, 47.
(34) Private communication with R. G. Forbes.